Targeting *Echinococcus multilocularis* PIM kinase for improving anti-parasitic chemotherapy

Akito Koike[1], Frank Becker[2], Peter Sennhenn[3], Jason Kim[4], Jenny Zhang[4], Stefan Hannus[2], Klaus Brehm[1,*]

[1]University of Würzburg, Institute of Hygiene and Microbiology, Consultant Laboratory for Echinococcosis, Würzburg, Germany

[2] Intana Bioscience GmbH, Martinsried, Germany

[3] transMedChem Consulting, München, Germany

[4]Immuneering Corporation, Cambridge, MA, USA

Short title: *Echinococcus multilocularis* PIM kinase

*Corresponding author.

Email: kbrehm@hygiene.uni-wuerzburg.de (KB)

Abstract

Background: The potentially lethal zoonosis alveolar echinococcosis (AE) is caused by the metacestode larval stage of the tapeworm *Echinococcus multilocularis*. Current AE treatment options are limited and rely on surgery as well as on chemotherapy involving benzimidazoles (BZ). BZ treatment, however, is parasitostatic only, must be given for prolonged time periods, and is associated with adverse side effects. Novel treatment options are thus urgently needed.

Methodology/Principal findings: By applying a broad range of kinase inhibitors to *E. multilocularis* stem cell cultures we identified the proto-oncogene PIM kinase as a promising target for anti-AE chemotherapy. The gene encoding the respective *E. multilocularis* ortholog, EmPIM, was characterized and *in situ* hybridization assays indicated its expression in parasite stem cells. By yeast two-hybrid assays we demonstrate interaction of EmPIM with *E. multilocularis* CDC25, indicating an involvement of EmPIM in parasite cell cycle regulation. Small molecule compounds SGI-1776 and CX-6258, originally found to effectively inhibit human PIM kinases, exhibited detrimental effects on *in vitro* cultured parasite metacestode vesicles and prevented the formation of mature vesicles from parasite stem cell cultures. To improve compound specificity for EmPIM, we applied a high throughput *in silico* modelling approach, leading to the identification of compound Z196138710. When applied to *in vitro* cultured metacestode vesicles and parasite cell cultures, Z196138710 proved equally detrimental as SGI-1776 and CX-6258, but displayed significantly reduced toxicity towards human HEK293T and HepG2 cells.

Conclusions/Significance:

Repurposing of kinase inhibitors initially designed to affect mammalian kinases for helminth disease treatment is often hampered by adverse side effects of respective compounds on human cells. Here we demonstrate the utility of high throughput *in silico* approaches to design small molecule compounds of higher specificity for parasite cells. We propose EmPIM as a promising target for respective approaches towards AE treatment.

Author summary

The larva of the tapeworm *E. multilocularis* grows tumor-like within the host liver, thus causing the lethal disease alveolar echinococcosis (AE). Anti-parasitic treatment relies on chemotherapy with benzimidazoles, which do not kill the parasite and must be applied for years. As druggable enzymes with key functions in growth control, protein kinases are promising drug targets and many kinase inhibitors have been identified during cancer research. Optimized for binding to human kinases, however, repurposing of such drugs for parasitic disease treatment is associated with adverse side effects. Herein, the authors applied an *in silico* approach to identify small molecule compounds that show higher specificity for a parasite kinase, EmPIM, over its mammalian homologs. The authors demonstrate expression of EmPIM in *Echinococcus* stem cells, which are the drivers of parasite growth, and show that mammalian PIM kinase inhibitors SGI-1776 and CX-6258 also affect parasite development *in vitro*. Finally, they show that one of the *in silico* screened compounds is equally effective against the parasite as SGI-1776 and CX-6258, but significantly less toxic to human cells. These results demonstrate the utility of *in silico* approaches to identify parasite-specific kinase inhibitors.

Introduction

The metacestode (MC) larval stage of the cestode *E. multilocularis* is the causative agent of alveolar echinococcosis (AE), a potentially lethal zoonosis prevalent in the Northern Hemisphere [1]. Intermediate hosts (rodents, humans) are infected by oral uptake of infectious eggs, which contain an embryonic larval stage, called the oncosphere. Within the intestine of the intermediate host, the oncosphere hatches from the egg, penetrates the intestinal barrier, and gains access to the inner organs. Usually within the host liver, the oncosphere then undergoes a metamorphosis-like transition towards the MC stage [2]. The *E. multilocularis* MC consists of numerous vesicles, which grow infiltratively, like a malignant tumour, into the surrounding liver tissue, eventually resulting in organ failure if no adequate treatment is applied [3]. As we have previously shown, MC growth and proliferation strictly depend on a population of pluripotent stem cells (called 'germinative cells' (GC) in the case of *Echinococcus*), which, as typical for flatworms, are the only mitotically active cells of the MC and give rise to all differentiated cells [4]. Currently, the only option to cure AE is surgical removal of the invading MC tissue, supported by chemotherapy using benzimidazoles (BZ; albendazole, mebendazole), which target parasite β-tubulin [5]. Surgical removal of parasite tissue is, however, only possible in around 20% of cases, leaving BZ chemotherapy as the only remaining treatment option for non-operable patients [3]. Although the prognosis of such patients has significantly improved after the introduction of BZ chemotherapy around 40 years ago, adverse side effects are frequently observed [6]. Furthermore, BZ are parasitostatic only and must be applied for years to decades, sometimes even life-long [7]. Since GC are the only mitotically active cells of the MC [4], it has already been proposed that the high recurrence rates after anti-AE chemotherapy are due to limited activity of BZ against the parasite's stem

cell department [8]. Hence, alternative drugs are urgently needed, which are also active against the *Echinococcus* GC [5].

Due to their catalytical process in transferring phosphate onto protein targets, protein kinases are particularly druggable enzymes [9] and most small molecule compounds that interfere with kinase activity bind to the ATP binding pocket [10]. Furthermore, protein kinases are crucially involved in regulating proliferation and differentiation of eukaryotic cells, making them highly attractive targets for strategies to chemically interfere with aberrant cell proliferation, e.g. in the context of malignant transformation [11]. One of these protein kinases, the PIM (proviral integration site for murine leukemia virus) kinase, has recently drawn much attention as a potential target for treating multiple forms of cancer [12–19]. Mammals typically express three PIM kinase isoforms, Pim-1, Pim-2, and Pim-3, which are constitutively active serine/threonine kinases [20] that phosphorylate numerous protein substrates and are downstream effectors of a variety of cytokine signalling pathways [21]. Via activation of CDC25 phosphatase, mammalian Pim-1 is involved in the regulation of the cell cycle [22,23] and aberrant expression of PIM kinases has been associated with numerous forms of malignant transformation [21]. A hallmark of PIM kinases is their unusual hinge region, which facilitates the development of specific kinase inhibitors and, during recent years, several small molecule compounds with activities against PIM kinases have been identified. Of these, the imidazole pyridazine compound SGI-1776 proved to be an effective pan-PIM inhibitor with IC_{50} values of 7, 363, and 69 nM against human Pim-1, Pim-2, and Pim-3, respectively, but also inhibited the kinases FLT3 (44 nM) and haspin (34 nM) [15]. Among second generation inhibitors, the oxindole-based compound CX-6258 displayed even higher specificity for PIM kinases than SGI-1776 (IC_{50} Pim-1, 5 nM; Pim-2, 25 nM, Pim-3, 16 nM) [24] and less activity against FLT3

(IC_{50}: 134 nM) [25]. At least in melanoma cell lines, CX-6258 also showed activities against haspin kinase, although also at much higher IC_{50} values than against Pim-1 and Pim-3 [26]. Although SGI-1776 has proceeded to clinical phase I trials against non-Hodgkin lymphoma and prostate cancer, the respective studies have been terminated due to toxicity in cardiac electric cycle prolongation [27], probably due to their activities against PIM kinases in non-cancer cells.

In the present work, we demonstrate that SGI-1776 and CX-6258 also exert detrimental effects on *in vitro* cultivated stem cells and larval stages of *E. multilocularis*. We characterized the *Echinococcus* PIM kinase ortholog, show that it contains the majority of amino acid residues that mediate the binding of PIM inhibitors to the ATP binding pocket, and demonstrate that, like the mammalian counterpart Pim-1, the *Echinococcus* enzyme interacts with CDC25 phosphatase. Using an *in silico* modelling approach to discriminate between mammalian and parasite PIM sequences, we then identified compound Z196138710, which displays equal toxicity against parasite larvae as SGI-1776 or CX-6258, but which is much less toxic for mammalian cells. The impact of these findings on drug design strategies against AE are discussed.

Methods

Ethics statement

In vivo propagation of parasite material was performed in mongolian jirds (*Meriones unguiculatus*), which were raised and housed at the local animal facility of the Institute of Hygiene and Microbiology, University of Würzburg. This study was performed in strict accordance with German (*Deutsches Tierschutzgesetz,TierSchG*, version from Dec-9-2010) and European (European directive 2010/63/EU) regulations on the

protection of animals. The protocol was approved by the Ethics Committee of the Government of Lower Franconia (Regierung von Unterfranken) under permit numbers 55.2–2531.01-61/13 and 55.2.2-2532-2-1479-8.

Organisms and culture methods

All experiments were performed with the *E. multilocularis* isolates H95 and GH09 [28] which either derive from a naturally infected fox of the region of the Swabian Mountains, Germany (H95) [29] or from Old World Monkey species (*Macaca fascicularis*) that had been naturally infected in a breeding enclosure (GH09) [30]The isolates were continuously passaged in mongolian jirds (*Meriones unguiculatus*) essentially as previously described [31,32]. *In vitro* culture of parasite metacestode vesicles (MV) under axenic conditions was performed as previously described [32] and the isolation and maintenance of *Echinococcus* primary cell cultures (PC) was carried out essentially as established by Spiliotis et al. [33]. In all cases, media were changed every three to four days (d). For inhibitor studies, specific concentrations of compounds, dissolved as 10-50 mM stock solutions and stored at -80°C, were added to parasite cultures as indicated and as negative control DMSO (0.1 %) was used. SGI-1776 was purchased from Selleckchem (Houston, Texas) and CX-6258 was from Cayman chemical (Ann Arbor, Michigan). Z196138710 was purchased from SIA Enamine (Riga, Latvia). Providers of other kinase inhibitors are listed in S1 Table. A6 medium was prepared by seeding 1.0×10^6 rat Reuber hepatoma cells [32] in 175 cm^2 culture flasks with 50mL DMEM (Dulbecco's Modified Eagle Medium) + GlutaMAX-I (life technologies) including 10% Fetal Bovine Serum Superior (life technologies) and incubated for 6 days under aerobic condition. The supernatant was sterile filtrated to remove hepatocytes. Similarly, B4 medium was prepared by seeding 1.0×10^7 rat

Reuber hepatoma cells in 175 cm^2 culture flasks with 50mL DMEM+GlutaMAX-I including 10% FBS and incubated for 4 days under aerobic conditions before sterile filtration.

Anti-parasitic inhibitor assays

In cell viability assays for initial screening of kinase inhibitors, PC were isolated from mature MV using a previously established protocol [33] and PC density was measured by densitometry. 1 Unit (U) of PC is defined as the amount which increases OD_{600} by 0.01. 15 U of isolated PC (～2.25 × 10^3 cells/well) were seeded into 384 well plates with 100 µl of conditioned medium (50% A6 medium + 50% B4 medium) including defined concentration of inhibitors as indicated. Plates were incubated at 37 °C under nitrogen atmosphere. After 3 d, cell viability was measured using the Cell Titer Glo 2.0 cell viability assay (Promega), according to the manufacturer's instructions. Luminescence was measured using a Spectramax iD3 Multi-mode Microplate reader (Molecular Devices; San Josè, CA, USA). Measured luminescence units were normalized to those of the DMSO control and visualized as heatmaps with GraphPad Prism version 9.3.1 (Graphpad software). All kinase inhibitors were tested independently in three technical replicates.

In mature MV assays, 10 individual MV each were cultured in 2 ml of conditioned medium (100% A6 medium) in the presence of inhibitors in 12 well plates under axenic conditions for 28 d as described in [34]. Structural integrity of MV was assessed using an optical microscope (Nikon eclipse Ts2-FL). Criteria for intact or damaged vesicles were essentially as previously described [35,36]. All experiments were performed using 3 biological replicates. Percentages of structurally intact vesicles were

189 statistically analyzed with one-way ANOVA with Dunnet's multiple comparison tests in
190 Graphpad prism 9.3.1(Graphpad software).
191 In vesicle formation assays, PC were isolated as described above and 100 U of
192 isolated PC (~ 1.5×10^4 cells/well) were seeded in 96 well plates with 200 µl of
193 conditioned medium (50% A6 medium + 50% B4 medium) for 21 d under nitrogen
194 atmosphere. The number of newly formed vesicles was counted using an optical
195 microscope (Nikon eclipse Ts2-FL) essentially as previously described [37] Kruskal-
196 Wallis test followed by Dunn's multiple comparisons test was used in GraphPad Prism
197 version 9.3.1(Graphpad software) to analyze the difference of vesicle numbers in
198 control and treatment groups. In this analysis, all concentrations were compared with
199 the negative control DMSO. Experiments with SGI-1776 and CX-6258 were performed
200 in three biological and technical replicates. Experiments with SGI-1776 and
201 Z196138710 were performed in three technical replicates.
202

203 **Mammalian cell cultivation and drug treatment**
204 The toxicity of inhibitors against mammalian cells was evaluated by treatment of the
205 commonly used cell lines HEK293T [38] and HepG2 [39], which were cultivated and
206 passaged as described in [40,41]. Semi-confluent cultured cells up to ten passages
207 after vial thawing were trypsinized and 1.0×10^3 cells were seeded in 384 well plates
208 with 50 µl of DMEM (Dulbecco's Modified Eagle Medium) + GlutaMAX-I (life
209 technologies) including 10% Fetal Bovine Serum Superior (life technologies). 24 h after
210 seeding, 50 µl of DMEM+GlutaMAX-I including FBS and inhibitors were added. Final
211 concentrations of inhibitors were adjusted to 0-30 µM as indicated, DMSO alone was
212 used as a control. Plates were incubated for 3 d under aerobic conditions and cell
213 viability was measured using the Cell Titer Glo 2.0 system (Promega) according to the

manufacturer's instructions. Luminescence was measured by a Spectramax iD3 Multi-mode Microplate reader (Molecular Devices). Three independent experiments with three technical replicates were carried out for both cell lines. Luminescence units were normalized to the DMSO control of each independent experiment and expressed as percentage of luminescence unit. One-Way-ANOVA test followed by Tukey's multiple comparisons test was used in GraphPad Prism version 9.3.1 (Graphpad software) for statistical analysis.

Nucleic acid isolation, cloning and sequencing

RNA isolation from *in vitro* cultivated axenic metacestode vesicles and primary cells was performed using a Trizol (5Prime, Hamburg, Germany)-based method as previously described [42]. For reverse transcription, 2 µg total RNA was used for cDNA synthesis using oligonucleotide CD3-RT (5'-ATC TCT TGA AAG GAT CCT GCA GGT_{26} V-3'). PCR products were cloned using the PCR cloning Kit (QIAGEN, Hilden, Germany) or the TOPO XL cloning Kit (Invitrogen). The complete list of primer sequences used for *empim* and *emcdc25* cDNA amplification and characterization is given in S2 Table. Upon cloning, PCR products were directly sequenced using primers binding to vector sequences adjacent to the multiple cloning site by Sanger Sequencing (Microsynth Seqlab, Göttingen, Germany). The sequences of all genes newly characterized in this work have been submitted to the GenBank, EMBL, and DDJB databases under accession numbers listed in S3 Table.

In situ hybridization and 5-ethynyl-2'-deoxyuridine (EdU) labeling

Digoxygenin (DIG)-labeled probes were synthesized by *in vitro* transcription with T7 and SP6 polymerase (New England Biolabs), using the DIG RNA labelling kit (Roche) according to the manufacturer's instructions from *empim*-cDNA fragments cloned into vector pJET1.2 (Thermo Fisher Scientific). Primers for probe production are listed in S2 Table. Probes were subsequently purified using the RNEasy Mini Kit (Qiagen), analysed by electrophoresis, and quantified by dot blot serial dilutions with DIG-labeled control RNA (Roche). Whole-mount *in situ* hybridization (WISH) was subsequently carried out on *in vitro* cultivated metacestode vesicles as previously described [4], using vesicles (isolate H95) of at least 1 cm in diameter to avoid losing material during washing steps. Fluorescent specimens were imaged using a Nikon Eclipse Ti2E confocal microscope and maximum projections created using ImageJ as previously described [43]. In all cases, negative control sense probes yielded no staining results. *In vitro* labelling with 50 µM EdU was done for 5, 8, or 16 hours (h) and fluorescent detection with Alexa Fluor 555 azide was performed after WISH essentially as previously described [4]. Series of pictures were taken at randomly chosen sections of the germinal layer of 5 MC vesicles with 40 × objective lens as Z-stack. Among the picture of each Z-stack, the layer of strongest signal was selected by the function of Z project in Fiji/ImageJ and processed [44]. EdU positive cells, WISH positive cells and double positive cells were counted manually and independently. The number of cells with each signal were calculated to cell number per mm^2 on the germinal layer.

Yeast Two hybrid (Y2H) analyses

The Gal4-based Matchmaker System (Takara Bio, USA) was used as described by Zavala-Góngora et al. [45,46] and Stoll et al [43]. Full-length cDNAs encoding EmPim

kinase and EmCdc25 phosphatase were PCR amplified from parasite cDNA using primers as listed in S2 Table and cloned into pGADT7 or pGBKT7 (Takara/Clontech). The *Saccharomyces cerevisiae* Gold strain (Clontech) was transformed with these plasmids by a one-step protocol described in Tripp et al. [47] and inoculated on Leu^-/Trp^- double dropout agarose plates. After incubation at 30 °C for 2 d, three colonies were picked from each transformation and inoculated independently in 2 ml of liquid Leu^-/Trp^- medium and incubated at 30 °C and 200 rpm until above OD_{660}=1.0. Yeast cultures were then diluted to equalized densities of OD_{660}=1.0, 0.1 and 0.01. Diluted yeast cultures were then dropped (5 µl each) onto Leu^-/Trp^-/His^- triple dropout plates and Leu^-/Trp^-/Ade^-/His^- quadruple dropout plates. After 48 - 72 h incubation at 30 °C, pictures of plates were taken with ProtoCOL SR colony counter (Synbiosis). The pictures were then converted into gray scale and processed using Fiji/imageJ [44] according to the protocol described in [48]. The level of growth on quadruple dropout plates with the inoculation density OD_{660}=1.0 was quantified as gray value. The quantified level of growth was statistically analysed with one-way ANOVA with Tukey's multiple comparison tests in Graphpad prism 9.3.1 (Graphpad software).

Bioinformatic procedures

Amino acid sequences of human Pim-1, Pim-2, Pim-3, Cdc25A, Cdc25B, and Cdc25C were used as queries in BLASTP searches against the *E. multilocularis* genome on Wormbase ParaSite [28,49,50]. Reciprocal BLASTP searches were performed again the SWISSPROT database as available under the KEGG database at Genomenet [51]. Dmain structure was analyzed with SMART8.0 [52–54]. Percent identity/percent similarity values of amino acid sequences were calculated through Sequence Manipulation Suite [55]. Multiple sequence alignments were performed using Clustal

omega [56] or CLUSTALW2.1 [57] in MEGA11 [58] under the following settings: Gap Opening Penalty = 10.00, Gap Extension Penalty = 0.20, Delay Divergent Cutoff = 30%. Aligned sequences were visualized by SnapGene Viewer (Snapgene software). Based on these alignments, phylogenic trees were generated by MEGA11. The statistical method for tree building was maximum likelihood, substitution model was Jones-Taylor-Thompson model, ML Heuristic method was Nearest-Neighbor Interchange. All transcripts of *Echinococcus* genes were analysed using Integrative Genomics Viewer [59,60] and previously published transcriptome data [28] to check for correct prediction of the sequences available through UniProt.

For virtual compound identification procedures, the target of interest (EmPim) was screened against Fluency, a proprietary deep learning-based platform [61]. The EmPim sequence tested was retrieved from Uniprot, functional domains were retrieved from the Pfam database. The target of interest was screened against 2 small molecule libraries: the Enamine Hinge Binders library [62] (n=24,000), and Enamine Diverse REAL drug-like library [63] version 2021q1-2, further filtered for drug-like properties based on Lipinski's rule of 5 [64] (n=21.4M). We applied predictions from 2 versions of the Fluency model, termed model 1 and model 2, which were trained on varying data sets and settings. Every combination of protein, compound library, and model was predicted by Fluency, resulting in 4 sets of predictions, ranking molecules from strongest predicted binder to weakest. Out of the 200 top-ranked *in silico* hits from the Fluency screen, 20 compounds were selected for purchase and profiling based on their Fluency Screen score, diversity of structures representing best the chemical space of the 200 hits and molecular modeling in hPIM (6VRU) employing seeSAR modeling software from BioSolveIT (version 11.2.). The generated poses were assessed for a

meaningful binding mode into the ATP-pocket, absence of intra- and intermolecular clashes and torsion quality.

Modeling of SGI-1776 and Z196138710 against human Pim-1 was performed using modeling software seeSAR Version 12.0.1 (BioSolveIT). To create broad diversity and to continue further, 200 poses were demanded within SeeSAR [65] per structure; the integrated Analyzer Mode was used to select those poses that were clash-free and only exhibited green torsions, i.e., torsions that are statistically prevalent in small-molecule crystal structures [66].

Results and Discussion

Initial screen of broad-range kinase inhibitors against *E. multilocularis* cell cultures

Based on sequence similarities between the catalytic domains and the presence of accessory domains, conventional protein kinases are basically divided into seven sub-groups, against which specific kinase inhibitors are available [67]. Homologs belonging to all these sub-groups are also expressed by *E. multilocularis* [28]. To identify kinase sub-groups that are important for *Echinococcus* stem cell function, we carried out an initial screen of 14 available kinase inhibitors covering all sub-groups, against *E. multilocularis* PC, which are strongly enriched in germinative (stem) cells [4] (Fig 1). To assess for direct cytotoxic effects, we performed cell viability assays with all inhibitors at a concentration of 10 μM and measured cell viability after 3 d of drug exposure. As shown in Fig 1, several inhibitors against the AGC and the CAMK groups showed clear effects against *Echinococcus* PC, whereas Dasatinib, directed against the BCR-Abl subfamily of tyrosine kinases, even stimulated parasite cell proliferation

334 under these conditions. The strongest anti-parasitic effect was achieved using the PIM-
335 specific inhibitor SGI-1776, with more than 50% growth inhibition after 3 d. In all further
336 experiments we therefore decided to concentrate on the PIM kinase family and their
337 role in *Echinococcus* stem cell biology.

338

339 **Fig 1. Activities of selected kinase inhibitors against *E. multilocularis* PC.** (A)
340 Phylogenetic tree of human protein kinases, based on homologies within the kinase
341 domain. Seven groups according to current nomenclature [68] are indicated. (B)
342 Heatmap showing the effects of different kinase inhibitors, covering all 7 groups, on *E.*
343 *multilocularis* PC. Colour-code below indicates levels of luminescence after 3 d of
344 incubation with 10 μM of inhibitor. Inhibitor names, human target proteins, and kinase
345 sub-families are indicated in the table to the left.

346

347 **Characterization of an *E. multilocularis* PIM kinase**

348 Since SGI-1776 was originally designed to inhibit human PIM kinases and showed
349 strong effects against *Echinococcus* PC, we were interested in characterizing parasite
350 PIM kinase orthologs. To this end, we performed BLASTP analyses using all three
351 human PIM isoforms as queries against the published *E. multilocularis* genome
352 sequence [28]. In all three cases we identified one single locus (EmuJ_000197100),
353 which encoded a protein with significant homologies. Reciprocal BLASTP analyses
354 against the SWISSPROT database using the EmuJ_000197100 gene product as a
355 query revealed high homologies to human Pim-1, particularly within the kinase domain
356 (47% identical, 65% similar residues) (Fig 2). Significant homologies were also
357 detected between the kinase domains of the EmuJ_000197100 gene product and

PRK2 (38%, 58%) and PSK2 (30%, 50%), which are PIM kinase orthologs of *Caenorhabditis elegans* and yeast, respectively. We thus named the *Echinococcus* gene *empim*, encoding the serine/threonine kinase EmPim (657 amino acids; 74 kDa theoretical MW). Since BLASTP searches against the *E. multilocularis* genome using the amino acid sequences of EmPim or all three human PIM kinase isoforms did not reveal any other gene with significant homologies, we concluded that *empim* is a single copy gene and that, in contrast to mammals, *E. multilocularis* only encodes one single PIM kinase isoform.

We then conducted similar analyses for the genome of the related trematode parasite *Schistosoma mansoni*, and, likewise, found one single locus (Smp_090890) encoding a PIM ortholog with significant homologies to EmPim, which we named SmPim (S1 Figure). The presence in the genome of just one gene encoding a PIM kinase ortholog appears to be a specific trait for parasitic flatworms since, as already mentioned, mammals express three PIM kinase isoforms [69,70]. Furthermore, three isoforms have already been described to be expressed by the related, but free-living, planarians, in which they belong to the group of ‘immediate early genes’, the expression of which is drastically upregulated during wound-induced responses [71]. Most interestingly, both EmPim and SmPim not only harbour the typical serine/threonine kinase domain but also a large C-terminal extension (S1 Figure), which is missing in human and planarian PIM kinase isoforms. Due to the absence of a regulatory domain, the human PIM kinase isoforms are considered constitutively active kinases, the activity of which is largely regulated at transcriptional, translation, and proteosomal degradation level [20,72]. Hence, in contrast to these enzymes, the PIM kinases of parasitic flatworms are likely subject to more elaborate regulatory mechanisms, although we could not

identify consensus regulatory regions, such as conserved phosphorylation sites, within the C-terminal extension.

Fig 2. Homologies and structural features of EmPim. (A) Amino acid sequence alignment of the kinase domains of human Pim-1 (HsPIM1), *E. multilocularis* Pim (EmPim), human FLT3 kinase (HsFLT3), human haspin kinase (HsHASPIN) and an *E. multilocularis* haspin kinase ortholog (EmHASPIN1). Residues identical to human Pim-1 are shown in black on grey. Kinase DFG motifs and the hinge regions are marked in red. Black triangles indicate residues known to be involved in the interaction between human Pim-1 and compound CX-6258 (numbered according to human Pim-1). (B) Presence of amino acid residues important for the interaction between human Pim-1 and CX-6258 in different kinases. For each of the 14 known residues of human Pim-1 (HsPIM1), the corresponding residue and position in *E. multilocularis* Pim (EmPIM), human FLT3 kinase (HsFLT3), human haspin kinase (HsHASPIN), and the *E. multilocularis* haspin kinase isoform (EmHASPIN1) are shown. Residues identical to those of human Pim-1 are marked in yellow, residues with similar biochemical properties are marked in green. The numbers of identical/similar residues compared to human Pim-1 are listed to the right as well as IC_{50} values of compounds CX-6258 and SGI-1776 to human enzymes.

Although the precise mode of interaction between SGI-1776 and PIM kinases is not known, crystallographic studies have already been conducted for the binding mode of CX-6258 to human Pim-1 [25]. These studies identified 14 amino acid residues of particular importance for the inhibitor-kinase interaction (indicated in Fig 2).

406 Interestingly, of these 14 residues, 10 are invariantly present in EmPim and two further
407 residues represent exchanges with conserved biochemical properties (Fig 2). In the
408 case of human FLT3 kinase, which is also inhibited to a certain extent by CX-6258,
409 only 7 of these residues are conserved (Fig 2). We thus propose that CX-6258 (and
410 most probably also SGI-1776) binds to EmPim with intermediate affinities when
411 compared to Pim-1 and FLT3. Notably, an FLT3 ortholog is apparently not expressed
412 by *E. multilocularis* since BLASTP genome mining using mammalian FLT3 as a query
413 did not reveal clear orthologs. This is supported by phylogenetic studies indicating that
414 FLT3 kinases have evolved before the chordate/urochordate split, but after the
415 divergence of protostomes and deuterostomes [73].

416 Apart from the tyrosine kinase FLT3, both SGI-17776 [15] and CX-6258 [26] have been
417 demonstrated to inhibit, although with lower affinities, the kinase *haspin* (haploid germ
418 cell-specific nuclear protein kinase), which mediates histone modification in mammals
419 [74]. Interestingly, a *haspin* ortholog is also expressed by the *E. multilocularis* genome
420 (EmuJ_000667600). Within the kinase domain, both the *Echinococcus* and the human
421 *haspin* kinases share 6 or 7, respectively, of the 14 residues involved in the CX-6258-
422 kinase interaction (Fig 2). It thus cannot be excluded that the parasite *Haspin* kinase
423 might also be targeted by CX-6258, at least to a certain extent.

424 Taken together, our analyses indicated that *E. multilocularis* expresses a single PIM
425 ortholog with substantial homologies to mammalian PIM kinases within the kinase
426 domain. Unlike PIM kinases of mammals or planarians, the PIM kinase enzymes of
427 parasitic flatworms contain a large C-terminal extension, indicating a more complex
428 mode of regulation than in the case of conventional (mammalian) PIM kinases. Based
429 on the conservation of the majority of amino acid residues that mediate binding of CX-
430 6258 to PIM kinases, we also concluded that available PIM kinase inhibitors should

primarily target EmPim in *Echinococcus* cells. We cannot rule out, however, that part of the effects of CX-6258 (and of SGI-1776) described below might be due to inhibition of the *Echinococcus haspin* ortholog.

Expression of *empim* in *Echinococcus* stem cells

In mammalian cells, PIM kinases are involved in cell proliferation and cell cycle regulation [75]. Since the germinative (stem) cell population is the only mitotically active *Echinococcus* cell type [4], we would expect expression of *empim* in germinative cells if EmPim has equivalent functions as mammalian PIM kinases. According to transcriptome analyses that had been produced during the *E. multilocularis* whole genome project [28], *empim* displayed higher expression in primary cell cultures after 2 d of incubation when compared to metacestode vesicles (S2 Figure). Since these cultures are highly enriched in germinative cells [4], we assumed that *empim* might show a dominant expression in this cell type. To clarify the situation, we carried out WISH analyses on MC vesicles that had been incubated with EdU, thus identifying the proliferating stem cell compartment. As shown in Fig 3, in the germinative layer of *in vitro* cultivated MV we detected *empim* signals in both EdU+ and EdU- cells. After an 8 h EdU pulse, around 25% of *empim*$^+$ cells were also EdU$^+$. For the majority of *empim*+ cells, however, we could not detect co-staining with EdU, indicating that they either represent post-mitotic, differentiated cells, or stem cells which were not in S-phase during the EdU pulse.

Fig 3. Expression of *empim* in *Echinococcus* MV. (A) WISH on *E. multilocularis* MV directed against *empim*. Channels shown are DAPI (blue, nuclear staining), WISH

(green, *empim*+), EdU (red, S-phase stem cells), and merge as indicated. Green arrow indicates example of *empim*+/EdU- cell, yellow arrow indicates example of *empim*+/EdU+ cell. Size bar represents 25 μm. (B) Statistical analysis of EdU+/*empim*+ staining patterns. Displayed are counted cell number per mm^2 of germinal layer in Z-stack analyses.

Previous studies on human chronic myelogenic leukemia cells indicated that Pim-1 is cell cycle-regulated with highest expression levels at G1-S and G2-M transitions, whereas a significant drop in Pim-1 expression occurs during S-phase [76]. Since EdU exclusively stains cells that have been in S-phase during the 8 h pulse, it is thus possible that the fraction of germinative cells which express *empim* is significantly higher than 25%, provided that the PIM kinase gene is also cell cycle-regulated in *Echinococcus*. In any case, our WISH/EdU experiments clearly indicate that a certain fraction of parasite stem cells expresses *empim*.

Interaction between EmPim and CDC25C phosphatase

Modulation of mammalian cell cycle progression through Pim-1 is mainly mediated by phosphorylation, and thereby activation, of dual specific phosphatases of the CDC25 family [22,23]. CDC25 phosphatases are highly conserved from yeast to mammals, are expressed in differing numbers of isoforms (e.g. 3 in humans, 1 in yeast, 2 in *Drosophila*, 4 in *C. elegans*), and induce the M-phase of the cell cycle by removing inhibitory phosphates from cyclin-dependent kinases [22,77,78]. Provided that EmPim, despite its unusual C-terminal extension, also mediates cell cycle progression in *Echinococcus*, we would expect that it physically interacts with CDC25 isoforms in this

parasite. To investigate these aspects, we first mined the available *E. multilocularis* genome sequence for the presence of CDC25 encoding genes. Using either of the three human CDC25 isoforms (CDC25A-C) as a query against the *E. multilocularis* genome in BLASTP analyses, we constantly identified one single locus (EmuJ_001174300) encoding a 762 amino acid (theoretical MW = 85,3 kDa) protein tyrosine phosphatase. The EmuJ_001174300 product displayed relatively weak overall homologies to CDC25 family members of humans, insects, or nematodes, but contained a Rhodanese domain, which is a hallmark of CDC25 family M-phase inducers [79] (Fig 4). Furthermore, amino acid residues within the Rhodanese domain that are critical for enzymatic function were highly conserved between the EmuJ_001174300 product and human CDC25 orthologs (Fig 4). Furthermore, in reciprocal BLASTP analyses against the SWISSPROT database using the EmuJ_001174300 gene product as a query, we detected highest homologies with CDC25 orthologs of mammals and invertebrate model organisms. We thus concluded that *E. multilocularis* genome contains a single locus encoding a CDC25 family phosphatase and named the respective gene *emcdc25* (encoding the protein EmCDC25).

Fig 4. Domain structure and homologies of EmCDC25. (A) Amino acid sequence alignment of the Rhodanese homology domains of EmCDC25 (EmCdc25), two *S. mansoni* CDC25 orthologs (SmCDC25A, SmCDC25B), and three human CDC25 orthologs (HsCDC25A-C). Conserved Rhodanese domain DCR motifs and the active site are indicated. Residues identical to EmCDC25 are shown in black on grey. (B) Phylogenetic tree based on Rhodanese domains of different CDC25-like phosphatases. Sequences derived from *E. multilocularis* (EmCDC25), *S. mansoni*

(SmCDC25A/B), *H. sapiens* (HsCDC25A-C), *C. elegans* (CeCDC25 1-4), *D. melanogaster* (TEW, STG), and *Saccharomyces cerevisiae* (MIH1). Statistical method for the tree was maximum likelihood (ML), substitution model was Jones-Taylor-Thompson, ML heuristic method was Nearest Neighbour Interchange. (C) Domain structures of EmCDC25, two different CDC25 orthologs of S.mansoni (SmCDC25A/B), and three human CDC25 isoforms (HsCDC25A-C). Shown are Rhodanese domains and M-phase inducer phosphatase domains, which are typical for mammalian isoforms.

To investigate possible interactions between EmPim and EmCDC25 we employed the yeast two-hybrid (Y2H) system which we had previously used to study protein-protein interactions between *Echinococcus* factors [43,45,46,80]. To this end, we cloned the full-length cDNAs for EmPim and EmCDC25 into vectors pGBKT7 and pGADT7, respectively, and assessed colony growth under medium (triple dropout plates) and high (quadruple dropout plates) stringency conditions. As shown in Fig 5, under medium stringency conditions we obtained growth for the combination EmPim-pGBKT7 x EmCDC25-pGADT7 but we also observed some growth capacity for EmPim-pGBKT7 with the empty vector control. Under high stringency conditions, on the other hand, only EmPim-pGBKT7 x EmCDC25-pGADT7 yielded positive results, indicating specific interaction between these proteins. Statistically significant differences between EmPim-pGBKT7 x EmCDC25-pGADT7 and empty vector controls were also observed in quantitative assays measuring yeast growth on quadruple dropout plates (OD660=1.0) (Fig 5). We thus concluded that, like in mammalian systems, the *Echinococcus* Pim kinase acts upstream of a CDC25 family phosphatase. Whether this interaction is involved in *Echinococcus* M-phase entry

529 control remains to be established. Due to the expression of EmPim in *Echinococcus*
530 stem cells and the high conservation of Pim/CDC25-dependent M-phase entry control
531 from yeast to mammals [22,23], such a role is, however, highly likely.

532

533 **Fig 5. Interaction between EmPim and EmCDC25.** (A) Representative pictures of
534 yeast transformant growth on plates selecting for plasmids (-Leu, -Trp) as well as triple
535 dropout (-Leu, -Trp, -His) and quadruple dropout (-Leu, -Trp, - His, -Ade) plates for
536 interaction under medium and high stringency conditions, respectively. Plasmid
537 combinations are indicated to the right, OD_{600} values for dropout density above. (B)
538 Quantitative assay measuring growth densities of yeast transformants. Plasmid
539 combinations are indicated below the graph. **** indicates $p \leq 0.0001$

540

541 We cannot yet tell whether the EmPim-EmCDC25 interaction indeed involves
542 phosphorylation of the M-phase regulator by the PIM kinase, although this is clearly
543 the case for human Pim-1 and CDC25A [23]. Currently available PIM kinase activity
544 assays rely on small peptide substrates basing on known target consensus sequences
545 (K/R-K/R-R-K/R-L-S/T-a; a = small amino acid residue) for human PIM kinases [81].
546 Unfortunately, we could not identify a sequence motif in EmCDC25 that exactly
547 matches the consensus of human PIM kinases, thus making it very difficult to establish
548 a functional EmPim kinase assay at present. Hence, further investigations are
549 necessary to clearly define phosphorylation sites for EmPim to facilitate kinase assays
550 e.g. for high throughput screening.

551

552 **Effects of SGI-1776 and CX6258 on *Echinococcus* larvae and stem cells**

553 Thus far, we had only measured effects of SGI-1776 on *Echinococcus* primary cells in
554 a cell viability assay. However, the actual target for anti-AE therapy are MC vesicles.
555 Furthermore, for effective elimination of parasite tissue, the capacity of stem cells to
556 differentiate into MV vesicles must be eliminated [5]. We thus employed in further
557 experiments previously established *in vitro* cultivation systems for mature MV and for
558 the production of MV from stem cells. Furthermore, since EmPim contained the
559 majority of residues that mediate the interaction between Pim kinases and CX-6258,
560 we also included this inhibitor in our analyses. As shown in Fig 6, both SGI-1776 and
561 CX-6258 had a detrimental and dose-dependent impact on the structural integrity of
562 mature MV. Although incubation of MV with 3 μM of both inhibitors for 28 d did not lead
563 to statistically significant effects, a concentration of 10 μM of these inhibitors led to a
564 drastic loss of structural integrity of all (CX-6258) or almost all (SGI-1776) vesicles (Fig
565 6). In the case of 3 μM of these inhibitors, many vesicles lost structural integrity but still
566 had the germinative layer attached to the parasite surface laminated layer (Fig 6). In
567 the case of 10 μM of both inhibitors, however, complete detachment of the parasite
568 tissue from the laminated layer was observed (Fig 6).

569

570 **Fig 6. Effects of SGI-1776 and CX-6258 on MV and PC.** (A) Inhibitor effects on
571 mature MV. *E. multilocularis* MV were incubated for 28 d in the presence of different
572 inhibitor concentrations as indicated below, and the number of structurally intact MV
573 was inspected microscopically. ** indicates $p \leq 0.0021$. (B) Representative examples
574 of MV incubated with different concentrations of inhibitors as indicated to the left. (C)
575 Inhibitor effectos on the formation of MV from PC. Parasite stem cell cultures were

incubated for 21 d in the presence of different inhibitor concentrations as indicated below. Numbers of fully mature MV were subsequently counted. * represents $p \leq 0.0332$.

Since even after loss of structural integrity, parasite vesicles can in theory still harbor living stem cells, we then tested both inhibitors for their capacity to affect the formation of MV from cultivated stem cells. As shown in Fig 6, both inhibitors affected MV formation from stem cells in a dose-dependent manner. In the case of SGI-1776, vesicle formation, which in this system is usually achieved after 21 d [32], was completely prevented in the presence of 30 μM SGI-1776, and almost completely in the presence of 10 μM. At 3 μM concentration, SGI-1776 did not lead to statistically significant effects. CX-6258, on the other hand, already drastically affected MV formation at 3 μM and completely inhibited MV development at higher concentrations (Fig 6).

Taken together, these analyses demonstrated clear detrimental effects of both PIM kinase inhibitors on *Echinococcus* larvae and stem cells. Based on the homologies of EmPim to human PIM kinases in regions that are important for inhibitor-kinase interaction (Fig 2), we concluded that most of these effects should be due to an inhibition of EmPim, although we cannot fully exclude that a certain degree of inhibition of the *Echinococcus haspin* kinase might have contributed.

In silico screening of EmPim inhibitors and effects against *Echinococcus* larvae

Due to their effects on human kinases, the utilization of currently available PIM inhibitors for chemotherapeutic approaches is associated with severe adverse effects [27,82–84]. At least in the case of SGI-1776, clinical trials against different forms of cancer had to be terminated since adverse effects on the cardiac electric cycle of patients were observed (NCT0084860, NCT01239108). We thus aimed at the identification of small molecule compounds that more specifically interact with the parasite enzyme isoforms when compared to human PIM kinases.

To this end, we first employed a very recently established *in silico* approach, the *Fluency* computational platform [60], which predicts quantitative binding affinities of compounds to target enzymes exclusively from amino acid sequences. Briefly, *Fluency* input consists of a protein amino acid sequence with domains optionally defined, and a small molecule structure in the form of SMILES. For each input-pair, *Fluency* predicts the protein-molecule binding affinity. Therefore, a natural application of *Fluency* is virtual screening of large molecular libraries against a target of interest to prioritize a top list of tractable size for downstream analysis such as medicinal chemistry analysis, docking, and experimental validation.

In a first *Fluency* screen of roughly 24 million compounds, using the EmPim amino acid sequence as a query, we obtained a list of 19,000 potential binders with predicted affinities between 10 nM and 1 μM for the parasite protein. Out of the 200 top-ranked *in silico* hits (S4 Table), 20 compounds were then selected for profiling based on (i) the *Fluency* screen score; (ii) diversity of chemical structures; and (iii) molecular modelling using the seeSAR software, thus assessing the ATP pocket binding mode as well as the absence of intra- and intermolecular clashes (S5 Table).

We then tested the 20 selected compounds against *E. multilocularis* MV and stem cells. First, we again employed the MV assay and found 4 of the compounds (Z30898879, Z196138710, Z65225039, Z354576500) being highly effective in inducing structural vesicle damage at concentrations of 3 and 10 μM (Fig 7). These 4 compounds were then employed in the PC vesicle formation assay, leading to the identification of compound Z196138710 which, at a concentration of 10 μM, completely prevented MV formation (Fig 7). Finally, we focussed on the thienopyrimidine Z196138710 (*N*-(4-(difluoromethoxy)-3-methoxybenzyl)-thieno-[3,2-*d*]-pyrimidin-4-amine) and tested it in comparison to SGI-1776 on mature MV and the PC cultivation system for MV development. As shown in Fig 7, a concentration of 10 μM Z196138710 led to structural disintegration of 100% of MV after 28 d, which was even more effective than SGI-1776. In the case of MV development from primary cells, Z196138710 showed effects similar to those of SGI-1776 (Fig 7).

Fig 7. Effects of Pim inhibitors on *Echinococcus* larvae and human cells. (A) Heat map showing the effects of 20 *in silico* screen compounds on MV. Different concentrations (indicated below) of each compound (indicated to the left) were incubated in vitro with MV for 28 d and structural integrity was assessed. Colour-code indicating percentages of surviving vesicles is indicated below. (B) Effects of four *in silico* screen compounds on MV production from PC. 10 μM of each compound (indicated below) were incubated for 21 d with PC *in vitro* and the production of MV was assessed. For comparison, SGI-1776 was tested at 10 μM. (C) Effects of Z196138710 and SGI-1776 on MV. Both compounds were tested at different concentrations (shown below) on MV *in vitro*. Structural integrity was measured after 28 d. P values less than 0.0001 are summarized with **** and p values less than 0.0332

are summarized with *. (D) Effects of Z196138710 and SGI-1776 on the *in vitro* formation of MV from PC. Both inhibitors were incubated at different concentrations (indicated below) for 21 d with PC and the formation of mature MV was measured. (E) Effects of Z196138710, SGI-1776, and CX-6258 on human HEK293T cells. HEK293T cells were incubated with different concentrations of inhibitors as indicated below. Cell viability was measured after 3 d. (F) Effects of inhibitors on human HepG2 cells. For experimental procedure, see (E). P values less than 0.0001 are summarized with **** and p values less than 0.0021 are summarized with **.

Effects of Pim inhibitors on human cell lines.

Having shown that Z196138710 shows similar (PC) or even higher (MV) toxicity towards *E. multilocularis* than SGI-1776, we were, in a final set of experiments, interested in possible toxicities of the thienopyrimidine compound on human cells. To this end, we employed the cell lines HEK293T and HepG2, which, according to previous studies, strongly depend on functional PIM kinases for cell viability [85-87]. As shown in Fig 7, at concentrations of 30 and 10 μM, both SGI-1776 and CX-6258 fully eliminated HEK293T and HepG2 cells within 3 d, whereas at the same concentrations, Z196138710 only inhibited both cell lines to 40-60% (Fig 7). At a concentration of 3 μM, the effects were even more drastic since SGI-1776 and CX-6258 still almost completely inhibited both cell lines whereas Z196138710 had no statistically significant effects (Fig 7). To assess whether the low toxicity of Z196138710 towards human cell lines was due to reduced binding of the thienopyrmidine compound to human PIM kinases, we finally performed *in silico* modelling assays of Z196138710 and SGI-1776 on the structure of Pim-1. As shown in S3 Figure, these analyses revealed a binding affinity of SGI-1776 in the nanomolar

range, which is in line with the results of previous biochemical assays [15]. For Z196138710, on the other hand, binding affinities in the micromolar range were obtained (S3 Figure), indicating that the low toxicity of the thienopyrimidine compound towards human cell lines is due to low binding to human PIM kinases. Although biochemical assays for measuring EmPim activity in the presence of kinase inhibitors will have to be established to verify these *in silico* analyses, our data at least point to Z196138710 as a promising candidate of an anti-*Echinococcus* compound with low adverse side effects.

In summary, we herein characterized an *E. multilocularis* single copy gene, which is expressed in the parasite's stem cell department, and which encodes a PIM kinase family member that interacts with an *Echinococcus* CDC25 ortholog in Y2H assays. These data at least point to a role of EmPim in *Echinococcus* cell cycle regulation, which appears to be one of the conserved functions of PIM kinases in vertebrate and invertebrate organisms [22,23,88]. An important role of EmPim in *Echinococcus* stem cell function is further supported by our data on the detrimental effects of known PIM kinase inhibitors, SGI-1776 and CX-6258, on *in vitro* cultivated MV and, particularly, PC, which are highly enriched in stem cells [4]. Since EmPim shares the majority of amino acid residues that are critical for inhibitor binding to mammalian Pim-1, it is highly likely that these effects are primarily due to the inhibition of EmPim, although a certain level of off-target effects, which might involve a parasite *haspin* ortholog, cannot be fully excluded. Since the germinative (stem) cells are the crucial cell type for parasite growth within the host [4], molecules that regulate their proliferative capacity are, *per se*, attractive targets for anti-parasitic chemotherapy, provided that small molecule compounds can be identified which discriminate between these factors and their (usually) highly conserved mammalian orthologs. In the case of *Echinococcus*,

high-throughput screening approaches towards the identification of specific inhibitory compounds from extensive small-molecule libraries are hampered by the fact that the complex conditions of parasite cultivation, particularly those for stem cell cultures, only allow parallel screening of dozens to maybe a few hundreds of molecules, and usually must be carried out over several weeks. Even though elegant approaches such as the PGI-assay for measuring MV integrity [89] or PC-based cell activity assays [90] allow compound screening against *E. multilocularis* in shorter time, a pre-selection of molecules from complex compound libraries is still necessary to narrow down screening procedures to manageable sizes. We herein combined a novel, target-based computational approach and *in silico* modeling techniques to select 20 compounds from complex libraries of roughly 24 million molecules. Of these 20 compounds, 4 displayed detrimental effects on *in vitro* cultivated parasite larvae and stem cells, and one of these, Z196138710, even out-matched known inhibitors against the target kinase family concerning side effects on human cells. Although the true capacity of Z196138710 in echinococcosis therapy still has to be established in future studies, particularly involving biochemical assays against Pim kinases and, of course, *in vivo* testing in murine models for echinococcosis [90], we propose the strategy employed in this study as highly effective in identifying promising candidates for downstream analyses towards this aim.

Acknowledgements

The authors wish to thank Monika Bergmann and Dirk Radloff for excellent technical assistance.

References

1. Romig T, Deplazes P, Jenkins D, Giraudoux P, Massolo A, Craig PS, et al. Ecology and Life Cycle Patterns of *Echinococcus* Species. Adv Parasitol. 2017;95:213–314.

2. Brehm K, Koziol U. *Echinococcus*-Host Interactions at Cellular and Molecular Levels. Adv Parasitol. 2017;95:147–212.

3. Kern P. Clinical features and treatment of alveolar echinococcosis. Curr Opin Infect Dis. 2010;23(5):505–12.

4. Koziol U, Rauschendorfer T, Zanon Rodríguez L, Krohne G, Brehm K. The unique stem cell system of the immortal larva of the human parasite *Echinococcus multilocularis*. Evodevo. 2014 Mar 6;5(1).

5. Brehm K, Koziol U. On the importance of targeting parasite stem cells in anti-echinococcosis drug development. Parasite. 2014;21.

6. Lightowlers MW, Gasser RB, Hemphill A, Romig T, Tamarozzi F, Deplazes P, u. a. Advances in the treatment, diagnosis, control and scientific understanding of taeniid cestode parasite infections over the past 50 years. Int J Parasitol. 2021;51(13–14):1167–92.

7. Brunetti E, Kern P, Vuitton DA, Writing Panel for the WHO-IWGE. Expert consensus for the diagnosis and treatment of cystic and alveolar echinococcosis in humans. Acta Trop. April 2010;114(1):1–16.

8. Schubert A, Koziol U, Cailliau K, Vanderstraete M, Dissous C, Brehm K. Targeting *Echinococcus multilocularis* stem cells by inhibition of the Polo-like kinase EmPlk1. PLoS Negl Trop Dis. 2014;8(6).

742 9. Pereira Moreira B, Weber MHW, Haeberlein S, Mokosch AS, Spengler B,
743 Grevelding CG, et al. Drug Repurposing and De Novo Drug Discovery of Protein
744 Kinase Inhibitors as New Drugs against Schistosomiasis. Molecules.
745 2022;27(4):1414.

746 10. Roskoski R. A historical overview of protein kinases and their targeted small
747 molecule inhibitors. Pharmacol Res. 2015 Oct;100:1–23.

748 11. Cicenas J, Zalyte E, Bairoch A, Gaudet P. Kinases and Cancer. Cancers.
749 2018;10(3):E63.

750 12. Chen WW, Chan DC, Donald C, Lilly MB, Kraft AS. Pim family kinases enhance
751 tumor growth of prostate cancer cells. Mol Cancer Res. 2005;3(8):443–51.

752 13. Asano J, Nakano A, Oda A, Amou H, Hiasa M, Takeuchi K, et al. The
753 serine/threonine kinase Pim-2 is a novel anti-apoptotic mediator in myeloma
754 cells. Leukemia. 2011;25(7):1182–8.

755 14. Nair JR, Caserta J, Belko K, Howell T, Fetterly G, Baldino C, et al. Novel
756 inhibition of PIM2 kinase has significant anti-tumor efficacy in multiple myeloma.
757 Leukemia. 2017;31(8):1715–26.

758 15. Chen LS, Redkar S, Bearss D, Wierda WG, Gandhi V. Pim kinase inhibitor, SGI-
759 1776, induces apoptosis in chronic lymphocytic leukemia cells. Blood.
760 2009;114:4150–7.

761 16. Lin YW, Beharry ZM, Hill EG, Song JH, Wang W, Xia Z, et al. A small molecule
762 inhibitor of Pim protein kinases blocks the growth of precursor T-cell
763 lymphoblastic leukemia/lymphoma. Blood. 2010;115(4):824–33.

764 17. Cohen AM, Grinblat B, Bessler H, Kristt DA, Kremer A, Shalom S, et al.
765 Increased expression of the hPim-2 gene in human chronic lymphocytic
766 leukemia and non-Hodgkin lymphoma. Leukemia and Lymphoma.
767 2004;45(5):951–5.

768 18. Brasó-Maristany F, Filosto S, Catchpole S, Marlow R, Quist J, Francesch-
769 Domenech E, et al. PIM1 kinase regulates cell death, tumor growth and
770 chemotherapy response in triple-negative breast cancer. Nat Med.
771 2016;22(11):1303–13.

772 19. Horiuchi D, Camarda R, Zhou AY, Yau C, Momcilovic O, Balakrishnan S, et al.
773 PIM1 kinase inhibition as a targeted therapy against triple-negative breast
774 tumors with elevated MYC expression. Nat Med. 2016;22(11):1321–9.

775 20. Qian KC, Wang L, Hickey ER, Studts J, Barringer K, Peng C, et al. Structural
776 basis of constitutive activity and a unique nucleotide binding mode of human
777 Pim-1 kinase. J Biol Chem. 2005;280(7):6130–7.

778 21. Arrouchi H, Lakhlili W, Ibrahimi A. A review on PIM kinases in tumors.
779 Bioinformation. 2019;15(1):40–5.

780 22. Bachmann M, Kosan C, Xing PX, Montenarh M, Hoffmann I, Möröy T. The
781 oncogenic serine/threonine kinase Pim-1 directly phosphorylates and activates
782 the G2/M specific phosphatase Cdc25C. Int J Biochem Cell Biol.
783 2006;38(3):430–43.

784 23. Mochizuki T, Kitanaka C, Noguchi K, Muramatsu T, Asai A, Kuchino Y. Physical
785 and functional interactions between Pim-1 kinase and Cdc25A phosphatase.

Implications for the Pim-1-mediated activation of the c-Myc signaling pathway. J Biol Chem. 1999;274(26):18659–66.

24. Haddach M, Michaux J, Schwaebe MK, Pierre F, O'Brien SE, Borsan C, et al. Discovery of CX-6258. A potent, selective, and orally efficacious pan-pim kinases inhibitor. ACS Med Chem Lett. 2012;3(2):135–9.

25. Bogusz J, Zrubek K, Rembacz KP, Grudnik P, Golik P, Romanowska M, et al. Structural analysis of PIM1 kinase complexes with ATP-competitive inhibitors. Sci Rep. 2017;7(1).

26. Melms JC, Vallabhaneni S, Mills CE, Yapp C, Chen JY, Morelli E, et al. Inhibition of haspin kinase promotes cell-intrinsic and extrinsic antitumor activity. Cancer Res. 2020;80(4):798–810.

27. Zhang X, Song M, Kundu JK, Lee MH, Liu ZZ. PIM Kinase as an Executional Target in Cancer. J Cancer Prev. 2018;23(3):109–16.

28. Tsai IJ, Zarowiecki M, Holroyd N, Garciarrubio A, Sanchez-Flores A, Brooks KL, et al. The genomes of four tapeworm species reveal adaptations to parasitism. Nature. 2013;496(7443):57–63.

29. Jura H, Bader A, Hartmann M, Maschek H, Frosch M. Hepatic tissue culture model for study of host-parasite interactions in alveolar echinococcosis. Infect Immun. 1996;64(9):3484–90.

30. Tappe D, Brehm K, Frosch M, Blankenburg A, Schrod A, Kaup FJ, et al. *Echinococcus multilocularis* infection of several Old World monkey species in a breeding enclosure. Am J Trop Med Hyg. 2007;77(3):504–6.

808 31. Spiliotis M, Tappe D, Sesterhenn L, Brehm K. Long-term in vitro cultivation of
809 *Echinococcus multilocularis* metacestodes under axenic conditions. Parasitol
810 Res. 2004;92(5):430–2.

811 32. Spiliotis M, Brehm K. Axenic in vitro cultivation of *Echinococcus multilocularis*
812 metacestode vesicles and the generation of primary cell cultures. Methods Mol
813 Biol. 2009;470:245–62.

814 33. Spiliotis M, Mizukami C, Oku Y, Kiss F, Brehm K, Gottstein B. *Echinococcus*
815 *multilocularis* primary cells: Improved isolation, small-scale cultivation and RNA
816 interference. Mol Biochem Parasitol. 2010;174(1):83–7.

817 34. Spiliotis M, Lechner S, Tappe D, Scheller C, Krohne G, Brehm K. Transient
818 transfection of *Echinococcus multilocularis* primary cells and complete in vitro
819 regeneration of metacestode vesicles. Int J Parasitol. 2008;38(8–9):1025–39.

820 35. Gelmedin V, Caballero-Gamiz R, Brehm K. Characterization and inhibition of a
821 p38-like mitogen-activated protein kinase (MAPK) from *Echinococcus*
822 *multilocularis*: Antiparasitic activities of p38 MAPK inhibitors. Biochem
823 Pharmacol. 2008;76(9):1068–81.

824 36. Hemer S, Brehm K. In vitro efficacy of the anticancer drug imatinib on
825 *Echinococcus multilocularis* larvae. Int J Antimicrob Agents. 2012;40(5):458–62.

826 37. Förster S, Koziol U, Schäfer T, Duvoisin R, Cailliau K, Vanderstraete M, et al.
827 The role of fibroblast growth factor signalling in *Echinococcus multilocularis*
828 development and host-parasite interaction. PLoS Negl Trop Dis. 2018;13(3).

829 38. DuBridge RB, Tang P, Hsia HC, Leong PM, Miller JH, Calos MP. Analysis of
830 mutation in human cells by using an Epstein-Barr virus shuttle system. Mol Cell
831 Biol. 1987;7(1):379–87.

832 39. Aden DP, Fogel A, Plotkin S, Damjanov I, Knowles BB. Controlled synthesis of
833 HBsAg in a differentiated human liver carcinoma-derived cell line. Nature.
834 1979;282(5739):615–6.

835 40. Pear WS, Nolan GP, Scott ML, Baltimore D. Production of high-titer helper-free
836 retroviruses by transient transfection. Proc Natl Acad Sci U S A.
837 1993;90(18):8392–6.

838 41. Aden DP, Fogel A, Plotkin S, Damjanov I, Knowles BB. Controlled synthesis of
839 HBsAg in a differentiated human liver carcinoma-derived cell line. Nature.
840 1979;282(5739):615–6.

841 42. Hemer S, Konrad C, Spiliotis M, Koziol U, Schaack D, Förster S, et al. Host
842 insulin stimulates *Echinococcus multilocularis* insulin signalling pathways and
843 larval development. BMC Biol. 2014;12:5.

844 43. Stoll K, Bergmann M, Spiliotis M, Brehm K. A MEKK1 – JNK mitogen activated
845 kinase (MAPK) cascade module is active in *Echinococcus multilocularis* stem
846 cells. PLoS Negl Trop Dis. 2021;15(12):e0010027.

847 44. Schindelin J, Arganda-Carreras I, Frise E, Kaynig V, Longair M, Pietzsch T, et
848 al. Fiji: an open-source platform for biological-image analysis. Nat Methods.
849 2012;9(7):676–82.

850 45. Zavala-Góngora R, Kroner A, Wittek B, Knaus P, Brehm K. Identification and
851 characterisation of two distinct Smad proteins from the fox-tapeworm
852 *Echinococcus multilocularis*. Int J Parasitol. 2003;33(14):1665–77.

853 46. Zavala-Góngora R, Derrer B, Gelmedin V, Knaus P, Brehm K. Molecular
854 characterisation of a second structurally unusual AR-Smad without an MH1
855 domain and a Smad4 orthologue from *Echinococcus multilocularis*. Int J
856 Parasitol. 2008;38(2):161–76.

857 47. Tripp JD, Lilley JL, Wood WN, Lewis LK. Enhancement of plasmid DNA
858 transformation efficiencies in early stationary-phase yeast cell cultures. Yeast.
859 2013;30(5):191–200.

860 48. Petropavlovskiy AA, Tauro MG, Lajoie P, Duennwald ML. A Quantitative
861 Imaging-Based Protocol for Yeast Growth and Survival on Agar Plates. STAR
862 Protoc. 2020;1(3):100182.

863 49. Howe KL, Bolt BJ, Shafie M, Kersey P, Berriman M. WormBase ParaSite − a
864 comprehensive resource for helminth genomics. Mol Biochem Parasitol.
865 2017;215:2–10.

866 50. Howe KL, Bolt BJ, Cain S, Chan J, Chen WJ, Davis P, et al. WormBase 2016:
867 Expanding to enable helminth genomic research. Nucl Acids Res.
868 2016;44(D1):D774–80.

869 51. Kanehisa M, Goto S, Kawashima S, Nakaya A. The KEGG databases at
870 GenomeNet. Nucl Acids Res. 2002;30(1):42–6.

871 52. Letunic I, Doerks T, Bork P. SMART: recent updates, new developments and
872 status in 2015. Nucl Acids Res. 2015;43:D257-60.

873 53. Letunic I, Khedkar S, Bork P. SMART: recent updates, new developments and
874 status in 2020. Nucl Acids Res. 2021;49:D458–60.

875 54. Letunic I, Bork P. 20 years of the SMART protein domain annotation resource.
876 Nucl Acids Res. 2018;46:D493–6.

877 55. Stothard P. The sequence manipulation suite: JavaScript programs for analyzing
878 and formatting protein and DNA sequences. Biotechniques. 2000;28(6):1102,
879 1104.

880 56. Madeira F, Pearce M, Tivey ARN, Basutkar P, Lee J, Edbali O, et al. Search and
881 sequence analysis tools services from EMBL-EBI in 2022. Nucleic Acids Res.
882 2022;gkay240.

883 57. Thompson JD, Higgins DG, Gibson TJ. CLUSTAL W: improving the sensitivity
884 of progressive multiple sequence alignment through sequence weighting,
885 position-specific gap penalties and weight matrix choice. Nucleic Acids Res.
886 1994;22(22):4673–80.

887 58. Tamura K, Stecher G, Kumar S. MEGA11: Molecular Evolutionary Genetics
888 Analysis Version 11. Mol Biol Evol. 2021;38(7):3022–7.

889 59. Thorvaldsdóttir H, Robinson JT, Mesirov JP. Integrative Genomics Viewer (IGV):
890 High-performance genomics data visualization and exploration. Brief Bioinform.
891 2013;14(2):178–92.

892 60. Robinson JT, Thorvaldsdóttir H, Winckler W, Guttman M, Lander ES, Getz G, et
893 al. Integrative genomics viewer. Nat Biotechnol. 2011;29(1):24–6.

894 61. Kim J, Zhang J, Cha Y, Kolitz S, Funt J, Chong RE, et al. Advanced
895 bioinformatics rapidly identifies existing therapeutics for patients with
896 coronavirus disease-2019 (COVID-19). J Transl Med. 2020;18(1):257.

897 62. Enamine. Hinge Binders Library [Internet]. [cited 2022 Feb 2]. Available from:
898 https://enamine.net/compound-libraries/targeted-libraries/kinase-library/hinge-
899 binders-library

900 63. Enamine. Real Compound Libraries [Internet]. https://enamine.net/compound-
901 collections/real-compounds/real-compound-libraries. [cited 2022 Feb 2].
902 Available from: https://enamine.net/compound-collections/real-compounds/real-
903 compound-libraries

904 64. Lipinski CA, Lombardo F, Dominy BW, Feeney PJ. Experimental and
905 computational approaches to estimate solubility and permeability in drug
906 discovery and development settings. Adv Drug Deliv Rev. 2001;46(1–3):3–26.

907 65. BioSolveIT GmbH SAG. SeeSAR version 12.1 [Internet]. 2022 [cited 2022 Jan
908 19]. Available from: www.biosolveit.de/SeeSAR

909 66. Schärfer C, Schulz-Gasch T, Hert J, Heinzerling L, Schulz B, Inhester T, et al.
910 CONFECT: conformations from an expert collection of torsion patterns.
911 ChemMedChem. 2013;8(10):1690–700.

912 67. Kanev GK, de Graaf C, de Esch IJP, Leurs R, Würdinger T, Westerman BA, et
913 al. The Landscape of Atypical and Eukaryotic Protein Kinases. Trends
914 Pharmacol Sci. 2019;40(11):818–32.

915 68. Hanks SK, Quinn AM, Hunter T. The protein kinase family: conserved features
916 and deduced phylogeny of the catalytic domains. Science. 1988;241(4861):42–
917 52.

918 69. Cuypers HT, Selten G, Quint W, Zijlstra M, Maandag ER, Boelens W, et al.
919 Murine leukemia virus-induced T-cell lymphomagenesis: integration of
920 proviruses in a distinct chromosomal region. Cell. 1984;37(1):141–50.

921 70. Konietzko U, Kauselmann G, Scafidi J, Staubli U, Mikkers H, Berns A, et al. Pim
922 kinase expression is induced by LTP stimulation and required for the
923 consolidation of enduring LTP. EMBO J. 1999;18(12):3359–69.

924 71. Wenemoser D, Lapan SW, Wilkinson AW, Bell GW, Reddien PW. A molecular
925 wound response program associated with regeneration initiation in planarians.
926 Genes Dev. 2012;26(9):988–1002.

927 72. Amaravadi R, Thompson CB. The survival kinases Akt and Pim as potential
928 pharmacological targets. J Clin Invest. 2005;115(10):2618–24.

929 73. Grassot J, Gouy M, Perrière G, Mouchiroud G. Origin and molecular evolution
930 of receptor tyrosine kinases with immunoglobulin-like domains. Mol Biol Evol.
931 2006;23(6):1232–41.

932 74. Dai J, Higgins JMG. Haspin: a mitotic histone kinase required for metaphase
933 chromosome alignment. Cell Cycle. 2005;4(5):665–8.

934 75. Morishita D, Katayama R, Sekimizu K, Tsuruo T, Fujita N. Pim kinases promote
935 cell cycle progression by phosphorylating and down-regulating p27kip1 at the
936 transcriptional and posttranscriptional levels. Cancer Res. 2008;68(13):5076–
937 85.

938 76. Liang H, Hittelman W, Nagarajan L. Ubiquitous expression and cell cycle
939 regulation of the protein kinase PIM-1. Arch Biochem Biophys. 1996;330(2):259–
940 65.

941 77. Chow JPH, Poon RYC, Ma HT. Inhibitory Phosphorylation of Cyclin-Dependent
942 Kinase 1 as a Compensatory Mechanism for Mitosis Exit. Mol Cell Biol.
943 2011;31(7):1478–91.

944 78. Donzelli M, Draetta GF. Regulating mammalian checkpoints through Cdc25
945 inactivation. EMBO Rep. 2003;4(7):671–7.

946 79. Bordo D, Bork P. The rhodanese/Cdc25 phosphatase superfamily. Sequence-
947 structure-function relations. EMBO Rep. 2002;3(8):741–6.

948 80. Hubert K, Zavala-Góngora R, Frosch M, Brehm K. Identification and
949 characterization of PDZ-1, a N-ERMAD specific interaction partner of the
950 *Echinococcus multilocularis* ERM protein Elp. Mol Biochem Parasitol.
951 2004;134(1):149–54.

952 81. Jacobs MD, Black J, Futer O, Swenson L, Hare B, Fleming M, et al. Pim-1 ligand-
953 bound structures reveal the mechanism of serine/threonine kinase inhibition by
954 LY294002. J Biol Chem. 2005;280(14):13728–34.

955 82. Raab MS, Thomas SK, Ocio EM, Guenther A, Goh YT, Talpaz M, et al. The first-
956 in-human study of the pan-PIM kinase inhibitor PIM447 in patients with relapsed
957 and/or refractory multiple myeloma. Leukemia. 2019;33(12):2924–33.

958 83. Cortes J, Tamura K, Deangelo DJ, de Bono J, Lorente D, Minden M, et al. Phase
959 I studies of AZD1208, a proviral integration Moloney virus kinase inhibitor in solid
960 and haematological cancers. Br J Cancer. 2018;118(11):1425–33.

961 84. Chen LS, Redkar S, Taverna P, Cortes JE, Gandhi V. Mechanisms of cytotoxicity
962 to Pim kinase inhibitor, SGI-1776, in acute myeloid leukemia. Blood.
963 2011;118(3):693–702.

964 85. Kronschnabl P, Grünweller A, Hartmann RK, Aigner A, Weirauch U. Inhibition of
965 PIM2 in liver cancer decreases tumor cell proliferation in vitro and in vivo
966 primarily through the modulation of cell cycle progression. Int J Oncol.
967 2020;56(2):448–59.

968 86. Peng C, Knebel A, Morrice NA, Li X, Barringer K, Li J, u. a. Pim kinase substrate
969 identification and specificity. J Biochem. 2007;141(3):353–62.

970 87. Yu Z, Zhao X, Ge Y, Zhang T, Huang L, Zhou X, u. a. A regulatory feedback
971 loop between HIF-1α and PIM2 in HepG2 cells. PLoS One. 2014;9(2):e88301.

972 88. Mihaylova Y, Abnave P, Kao D, Hughes S, Lai A, Jaber-Hijazi F, et al.
973 Conservation of epigenetic regulation by the MLL3/4 tumour suppressor in
974 planarian pluripotent stem cells. Nat Commun. 2018;9(1):3633.

975 89. Stadelmann B, Scholl S, Müller J, Hemphill A. Application of an in vitro drug
976 screening assay based on the release of phosphoglucose isomerase to
977 determine the structure-activity relationship of thiazolides against *Echinococcus*
978 *multilocularis* metacestodes. J Antimicrob Chemother. 2010;65(3):512–9.

979 90. Lundström-Stadelmann B, Rufener R, Ritler D, Zurbriggen R, Hemphill A. The
980 importance of being parasiticidal… an update on drug development for the
981 treatment of alveolar echinococcosis. Food Waterborne Parasitol.
982 2019;15:e00040.

983

Supporting information Captions

S1 Table. Providers of small molecule compounds and inhibitors used in this study.

S2 Table. Sequences of primers used in this study.

S3 Table. Accession numbers of genes and proteins analysed in this study.

S4 Table. Top 200 list of compounds after Fluency *in silico* screening against EmPim.

S5 Table. Structures and features of 20 compounds selected after Fluency *in silico* screening.

S1 Figure. Structural features and homologies of EmPim and SmPim.

S2 Figure. Expression of *empim* in PC and MV.

S3 Figure. SeeSAR analysis of SGI-1776 and Z196138710 binding to human Pim-1.

A

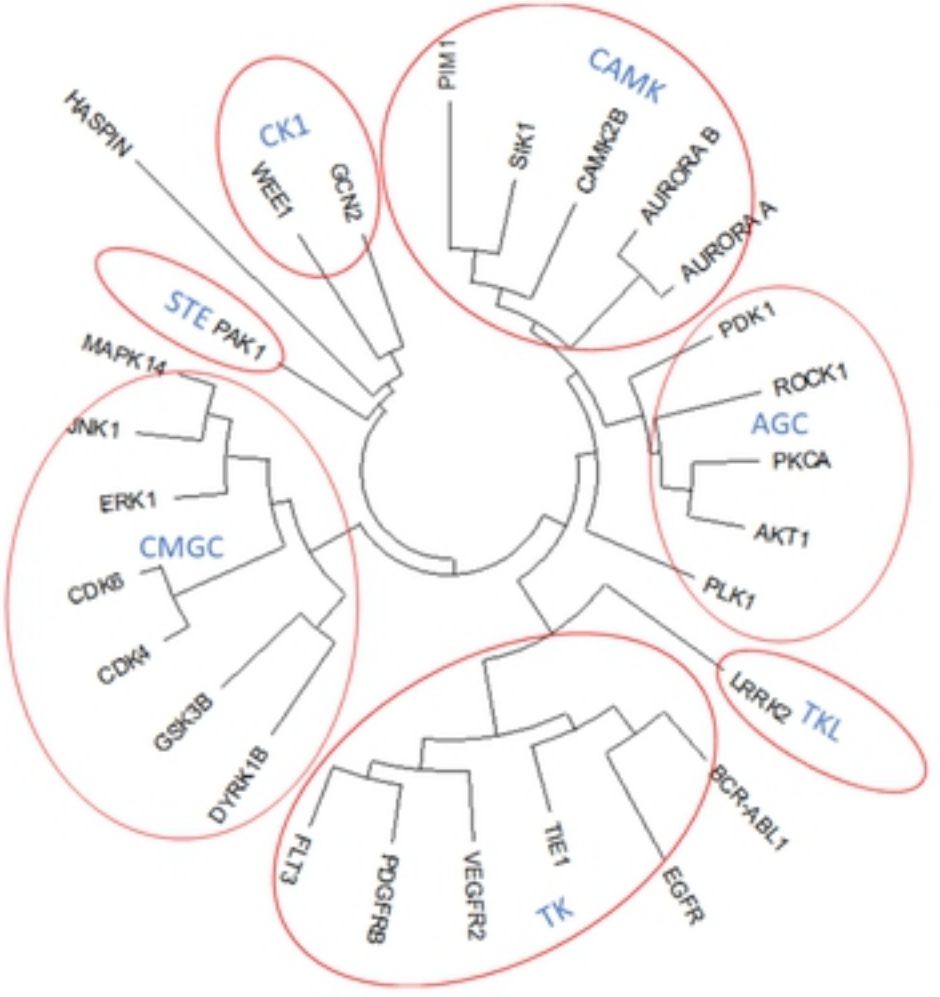

B

Group	Target	Inhibitor
AGC	PDK1	BX-912
AGC	PKC	Sotrastaurin
AGC	ROCK	Y-27632
CAMK	CaM II	KN-62
CAMK	PIM	SGI-1776
CAMK	Aurora A	Tozasertib
CK1	Wee1	Advosertib
CMGC	DYRK1B	AZ-191
CMGC	GSK-3	CHIR-99021
CMGC	ERK1, JNK, p38a	Tanzisertib
STE	PAK	FRAX597
TK	BCR-ABL	Dasatinib
TK	TIE	Cabozantinib
TKL	LRRK2	GNE-0877

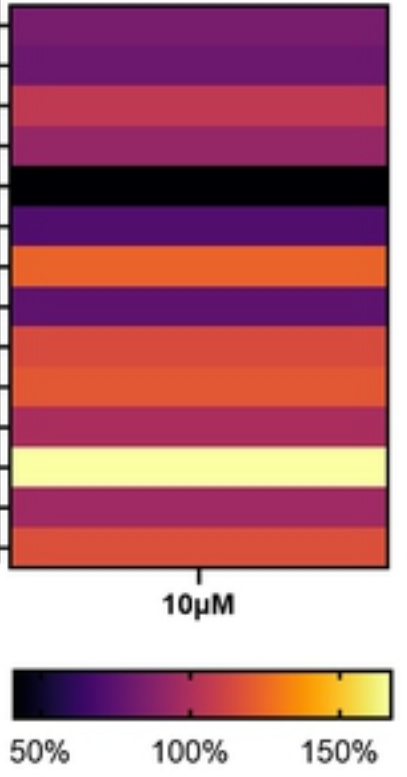

Fig 1

A

B

															identical residues	similar residues	IC_{50} of CX-6258(nM)	IC_{50} of SGI-1776(nM)
HsPIM1	L44	F49	V52	A65	K67	E89	I104	L120	V126	D128	D131	L174	I185	D186	14	0	5	7
EmPIM	V56	F61	V64	V77	K79	E101	S114	M130	V137	D139	D144	L185	I196	D197	10	2		
HsFLT3	L616	F621	V624	V637	I639	E661	V675	F718	S762	D764	E769	L818	C828	D829	7	3	134	44
HsHASPIN	I490	F495	V498	K511	F513	E535	I557	N581	I601	L603	E608	L656	I686	D687	7	3		34
EmHASPIN1	I299	Y304	V307	K317	F319	E341	I364	E388	M408	L410	D415	L461	I491	D492	7	1		

Fig 2

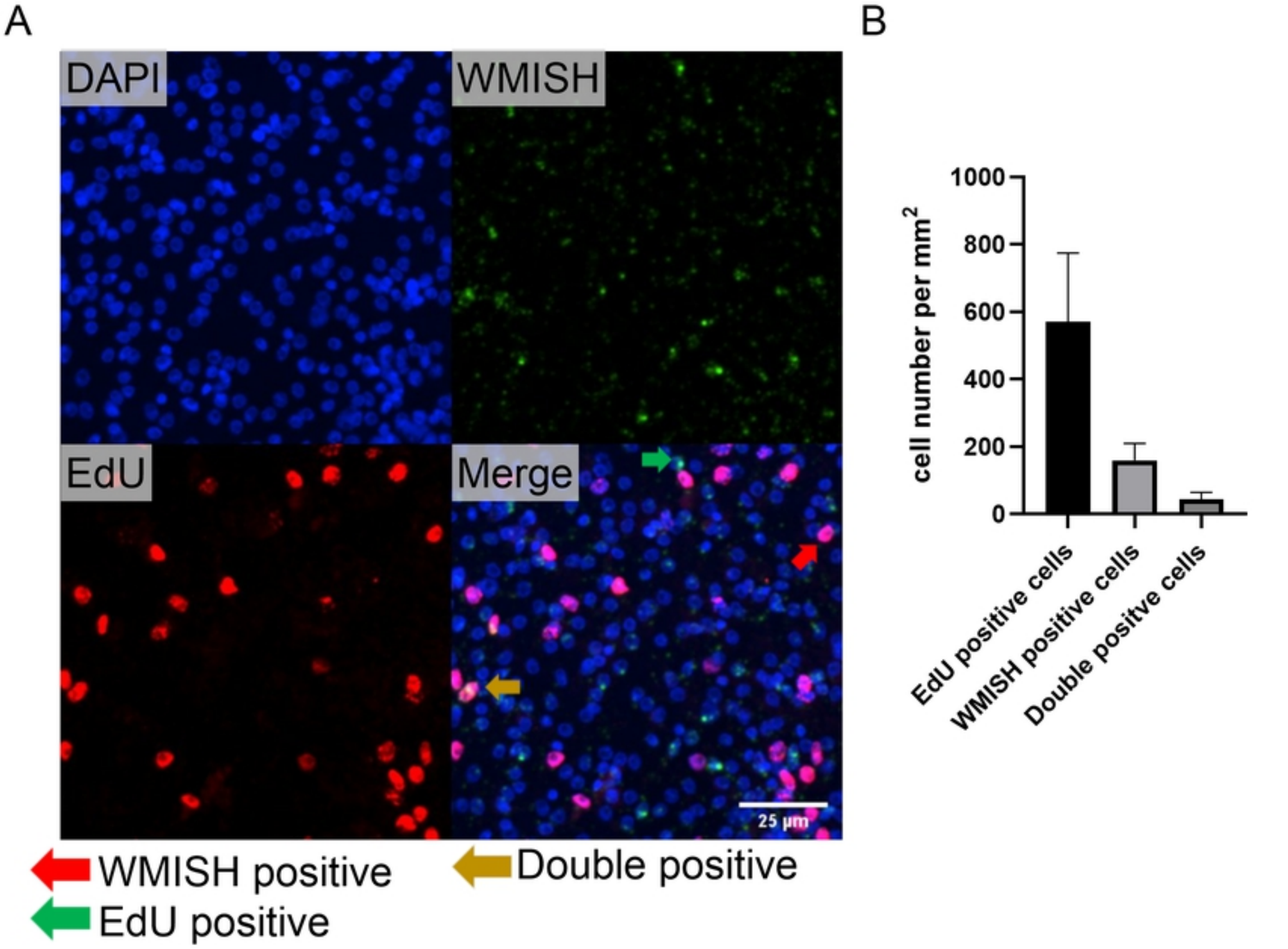
A
DAPI
WMISH
EdU
Merge
25 µm
WMISH positive
Double positive
EdU positive
B
cell number per mm2
1000
800
600
400
200
0
EdU positive cells
WMISH positive cells
Double positive cells

Fig 3

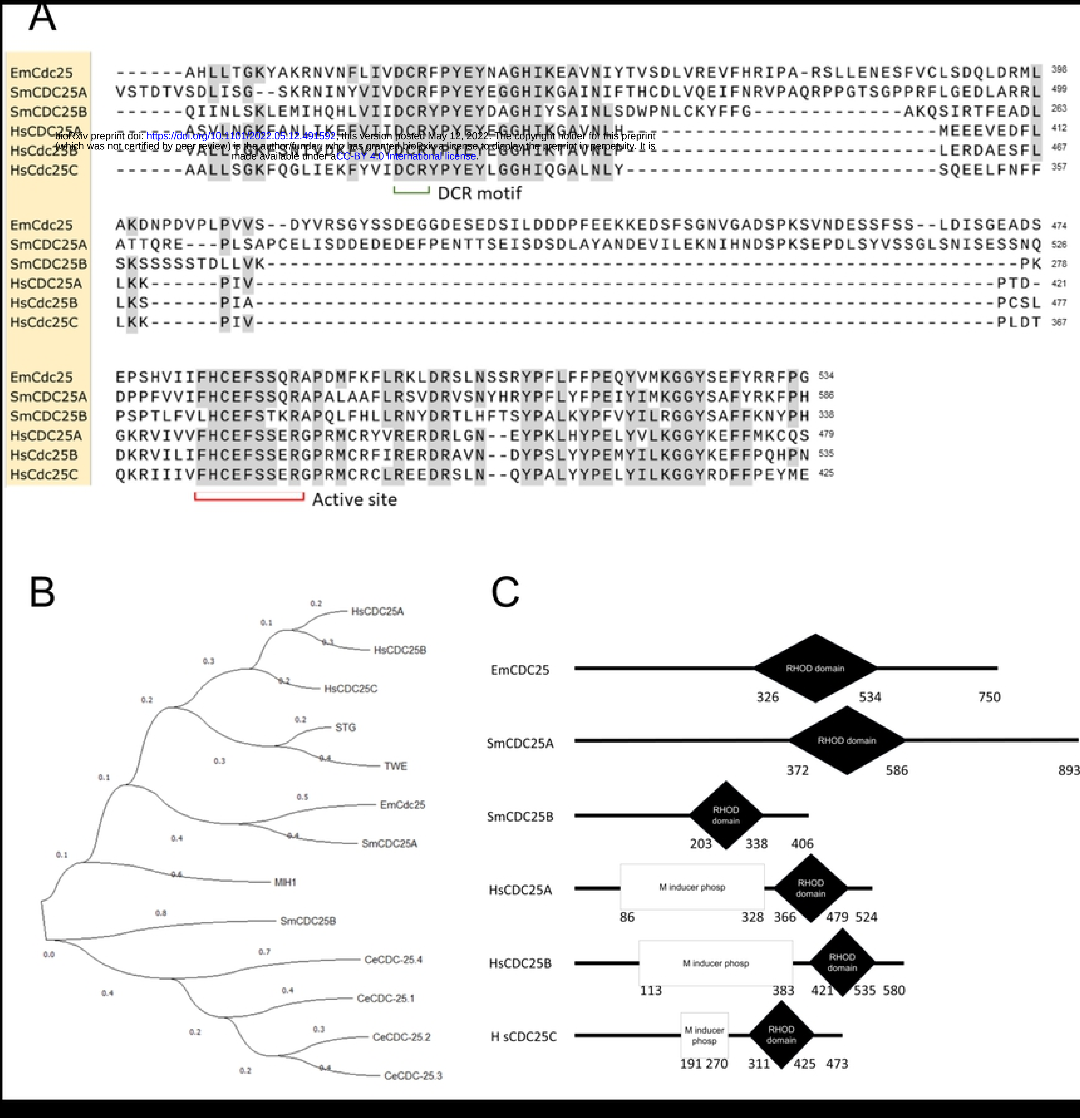

Fig 4

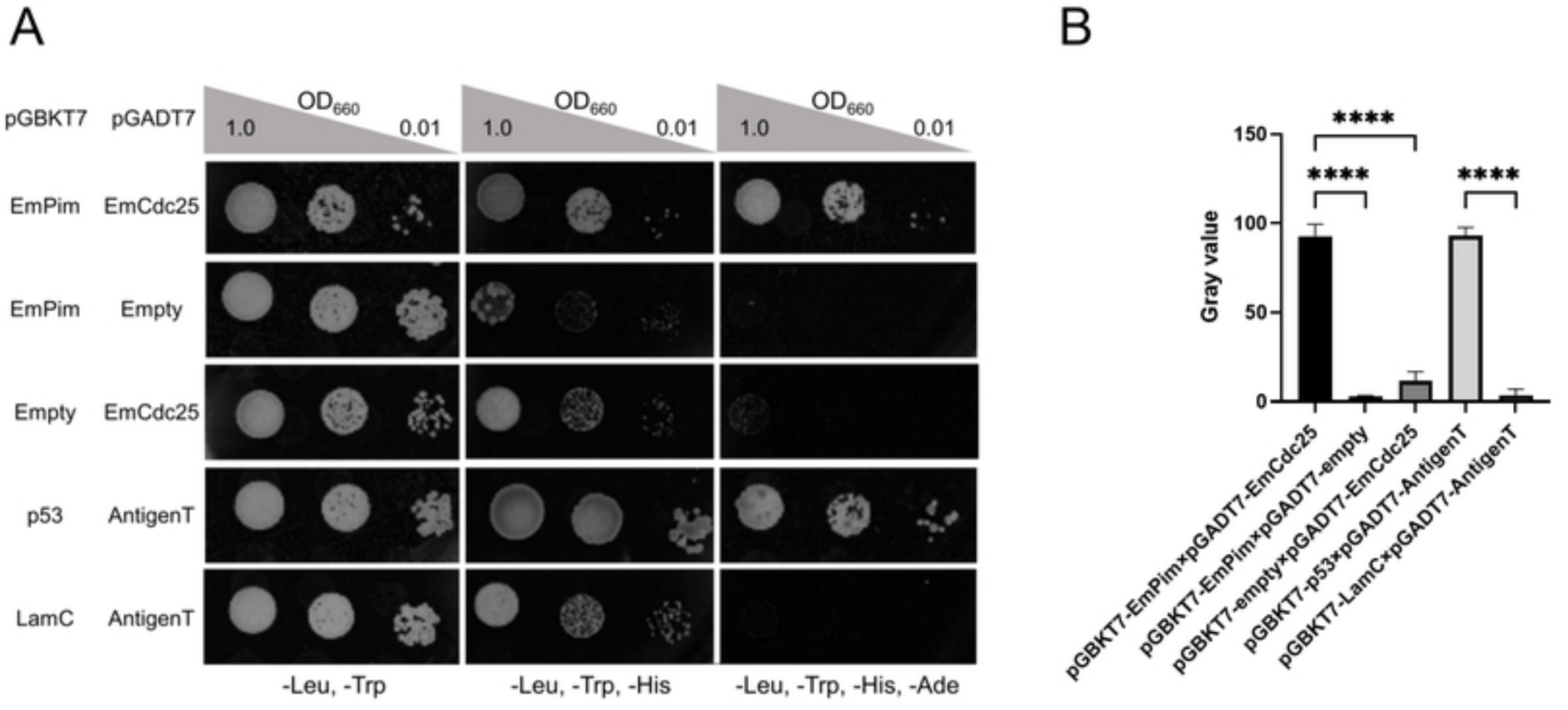
A
pGBKT7
pGADT7
OD660
1.0
0.01
EmPim
EmCdc25
EmPim
Empty
Empty
EmCdc25
p53
AntigenT
LamC
AntigenT
-Leu, -Trp
-Leu, -Trp, -His
-Leu, -Trp, -His, -Ade
B
Gray value
150
100
50
0
****
****
****
pGBKT7-EmPim×pGADT7-EmCdc25
pGBKT7-EmPim×pGADT7-empty
pGBKT7-empty×pGADT7-EmCdc25
pGBKT7-p53×pGADT7-AntigenT
pGBKT7-LamC×pGADT7-AntigenT

Fig 5

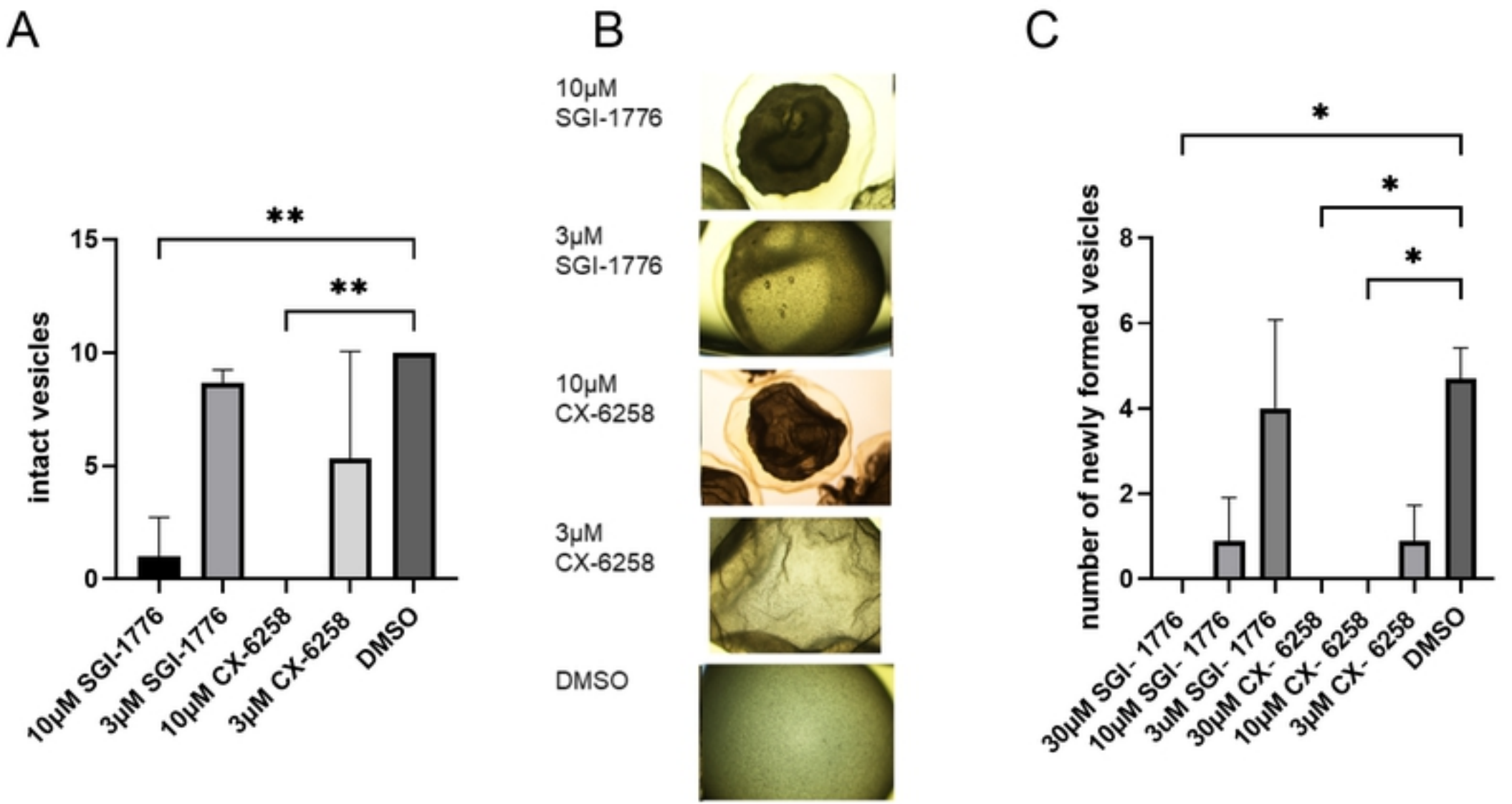
A
B
C
intact vesicles
15
10
5
0
**
**
10μM SGI-1776
3μM SGI-1776
10μM CX-6258
3μM CX-6258
DMSO
10μM SGI-1776
3μM SGI-1776
10μM CX-6258
3μM CX-6258
DMSO
number of newly formed vesicles
8
6
4
2
0
*
*
*
30μM SGI- 1776
10μM SGI- 1776
3uM SGI- 1776
30μM CX- 6258
10μM CX- 6258
3μM CX- 6258
DMSO

Fig 6

A

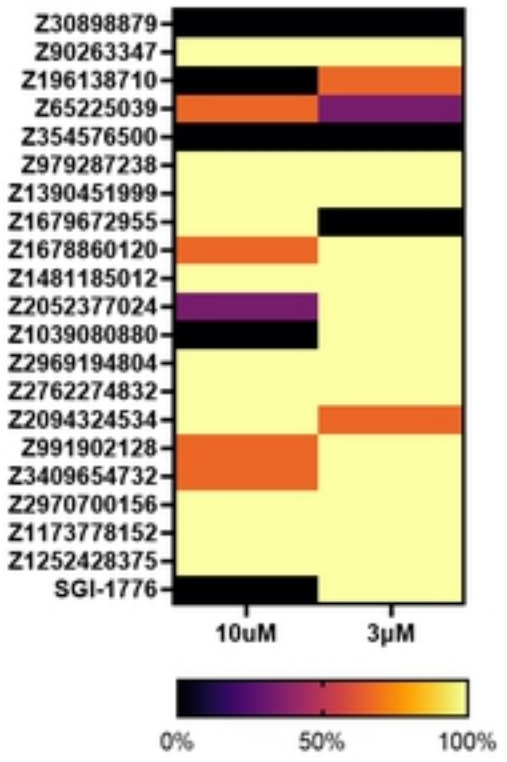
Z30898879
Z90263347
Z196138710
Z65225039
Z354576500
Z979287238
Z1390451999
Z1679672955
Z1678860120
Z1481185012
Z2052377024
Z1039080880
Z2969194804
Z2762274832
Z2094324534
Z991902128
Z3409654732
Z2970700156
Z1173778152
Z1252428375
SGI-1776
10uM
3μM
0%
50%
100%

B

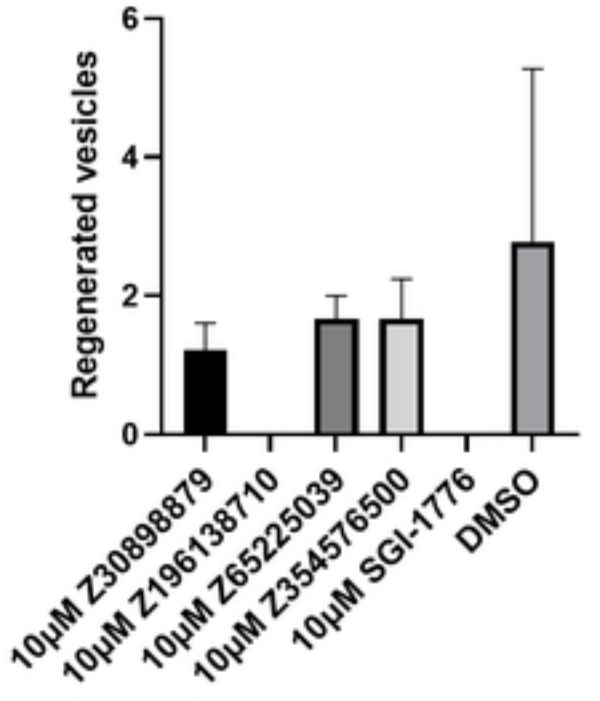
Regenerated vesicles
0
2
4
6
10μM Z30898879
10μM Z196138710
10μM Z65225039
10μM Z354576500
10μM SGI-1776
DMSO

C

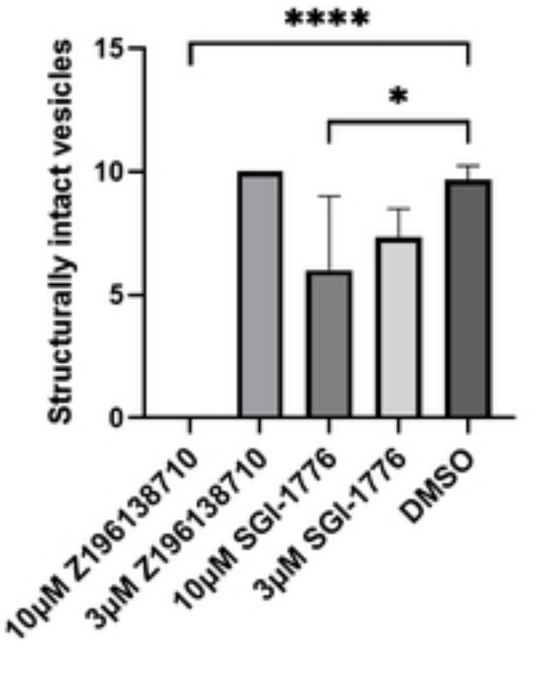
****
*
Structurally intact vesicles
0
5
10
15
10μM Z196138710
3μM Z196138710
10μM SGI-1776
3μM SGI-1776
DMSO

D

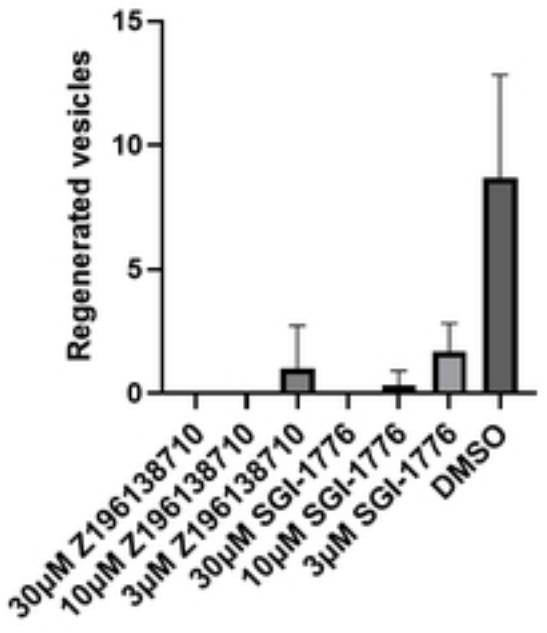
Regenerated vesicles
0
5
10
15
30μM Z196138710
10μM Z196138710
3μM Z196138710
30μM SGI-1776
10μM SGI-1776
3μM SGI-1776
DMSO

E

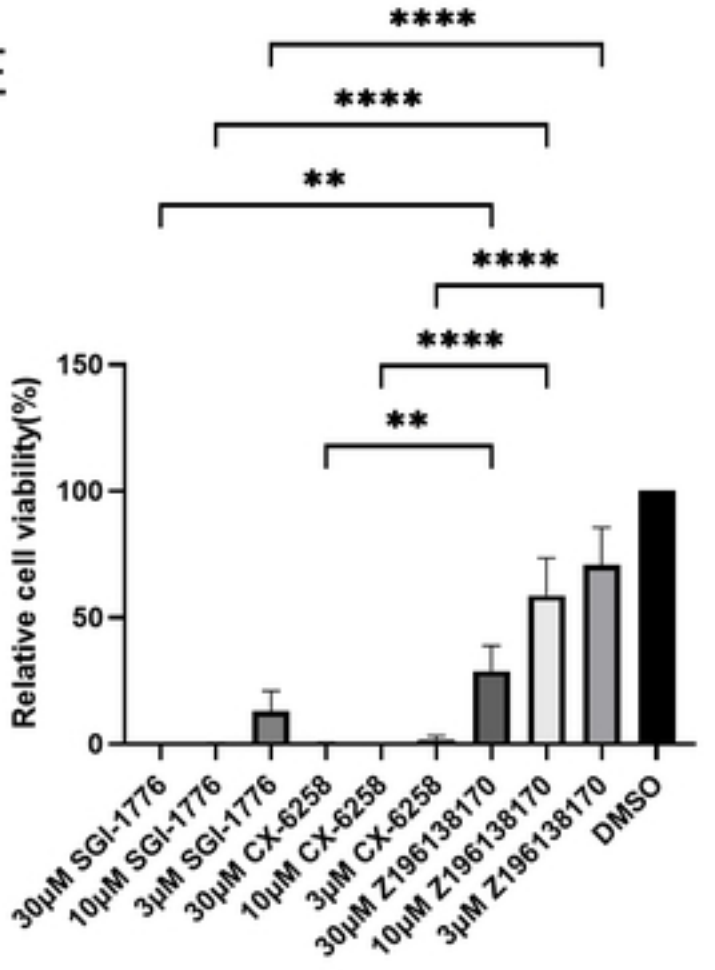
****
****
**
****
****
**
Relative cell viability(%)
0
50
100
150
30μM SGI-1776
10μM SGI-1776
3μM SGI-1776
30μM CX-6258
10μM CX-6258
3μM CX-6258
30μM Z196138170
10μM Z196138170
3μM Z196138170
DMSO

F

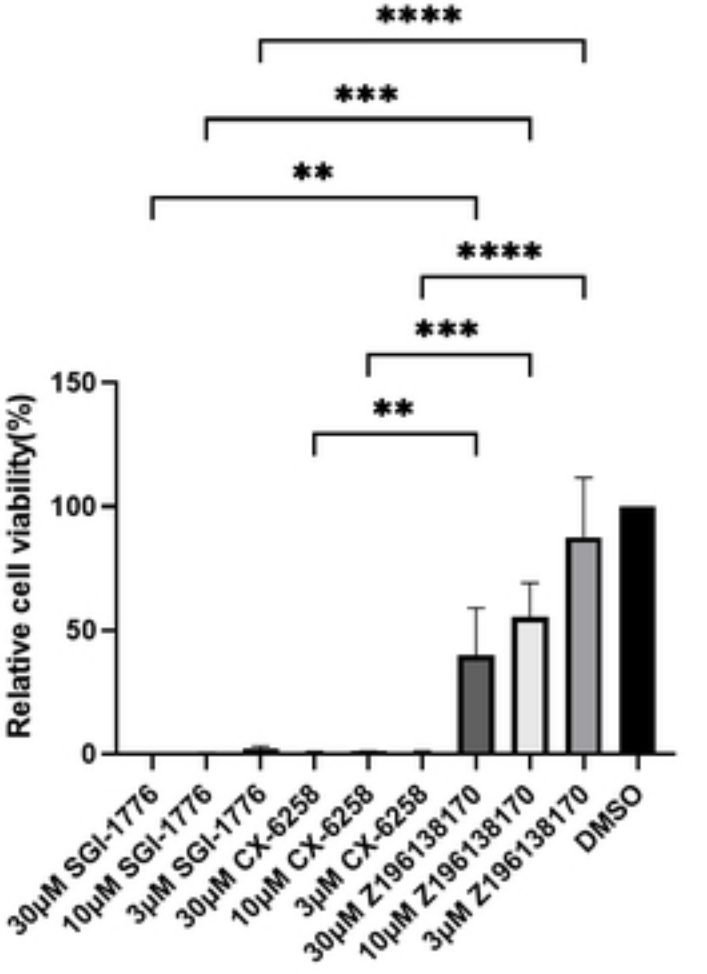
****
***
**
****
***
**
Relative cell viability(%)
0
50
100
150
30μM SGI-1776
10μM SGI-1776
3μM SGI-1776
30μM CX-6258
10μM CX-6258
3μM CX-6258
30μM Z196138170
10μM Z196138170
3μM Z196138170
DMSO

Fig 7